HTML ABSTRACT + LINKS

JOURNAL OF APPLIED PHYSICS VOLUME 96, NUMBER 1 1 JULY 2004

Modeling and measurement of surface displacements in $BaTiO_3$ bulk material in piezoresponse force microscopy

F. Felten and G. A. Schneider
Advanced Ceramics Group, Technical University of Hamburg-Harburg, 21073 Hamburg, Germany

J. Muñoz Saldaña
Centro de Investigación y de Estudios Avanzados del IPN, Unidad Querétaro, Libramiento Norponiente No. 2000, Fraccionamiento Real de Juriquilla, Querétaro 76230, Mexico

S. V. Kalinin
Oak Ridge National Laboratory, Condensed Matter Sciences Division, Oak Ridge, Tennessee 37831

(Received 22 December 2003; accepted 10 April 2004)

Piezoresponse force microscopy (PFM) is applied to image ferroelastic formed *c* domains in a single crystal ferroelectric barium titanate bulk material. A simple model and an analytical approach are presented, which provides a basis to understand the complex tip-surface interactions responsible for the image contrast in PFM. In particular, the measured amplitude of the piezoresponse out-of-plane surface displacements of a C^- domain is compared with theoretical results based upon a three-dimensional Green's function solution. The electric field distribution in the tip-surface contact is determined using image-charge calculations for a spherical tip separated by a thin water layer from a mechanically isotropic and electrically anisotropic dielectric half plane. © *2004 American Institute of Physics.* [DOI: 10.1063/1.1758316]

I. INTRODUCTION

The atomic force microscopy (AFM) piezoresponse mode, also called piezoresponse force microscopy (PFM), has been demonstrated to be a powerful tool to image ferroelectric domains in copolymer films, barium titanate, and lead zirconate titanate ceramics and thin films.[1–8] Applying an alternating voltage to a conductive AFM tip in contact with a piezoelectric specimen induces mechanical vibrations in the specimen, which can be demodulated with conventional lock-in techniques. These vibrations arise due to the converse piezoelectric effect and hence depend on the orientation of the polarization vector. The tip therefore represents a nanometer-sized movable top electrode probing the polarization distribution.

A qualitative explanation for the main contrast mechanism is shown in Fig. 1. It is based on the piezoelectricity of $BaTiO_3$ at room temperature having tetragonal distorted unit cells, i.e., the symmetry class 4mm. Considering a *c* domain under unconstraint conditions having a polarization vector perpendicular to the surface, a homogenous electric field parallel to the polarization vector, $E_3>0$, causes an expansion of the crystal in x_3 direction ($\varepsilon_3=d_{33}E_3$) and a contraction in *a* direction ($\varepsilon_1=\varepsilon_2=d_{31}E_3$), Fig. 1(b) (bottom). The same electric field leads to shear strains when applied to an unconstraint *a* domain, i.e., $\varepsilon_5=2\varepsilon_{31}=d_{15}E_1$, Fig. 1(a) (bottom). Transferred to the inhomogeneous electric field distribution of the small tip-sample contact area, the main component of the field leads to surface displacements indicated in Fig. 1 (top). Using an alternating voltage the electric field changes its direction periodically and the corresponding surface vibration is transferred to the tip. Thus, the out-of-plane and in-plane component can be quantified by analyzing the deflection and torsion signal, respectively.

Analytical approaches to describe special aspects of image contrast in PFM with the interaction between a small tip and a ferroelectric surface have been already presented.[9,10] For instance, Kalinin and Bonnell[9] used an analytical method to quantify the relative magnitudes of the electrostatic and electromechanical contributions to PFM interaction for C^+ and C^- domains in tetragonal ferroelectrics. As for the present paper, the analytical description of the electrostatic field distribution interior to the material underneath the tip-sample contact area is carried out using the image charge method for a dielectric material in consideration of the tip radius and the tip-surface separation.

However, to describe the contrast formation in PFM the piezoelectric surface displacement generated by the electromechanical interaction is needed. For instance, Karapetian *et al.*[11] present a piezoelectric Green's function solution for a point electric charge on top of a transversely isotropic half plane to calculate the corresponding surface displacements. In the present paper, instead of using a point charge a sphere with given electrical potential is used to model the AFM tip. The material is assumed as a transverse isotropic infinite *c* domain and the corresponding electrostatic field distribution interior to the material generated by the sphere is computed using a given analytical solution. Afterwards, the generated displacement field due to the converse piezoelectric effect is computed for different tip radii and tip-sample separations using a three-dimensional Green's function solution for an isotropic linear elastic dielectric containing piezoelectric eigenstrains. Due to the small piezoelectric coefficients of $BaTiO_3$, this approximation is assumed to be close to the coupled piezoelectric result. Finally, the surface displacements responsible for PFM contrast are calculated and com-

 © 2004 American Institute of Physics

Downloaded 20 Oct 2004 to 128.219.12.140. Redistribution subject to AIP license or copyright, see http://jap.aip.org/jap/copyright.jsp

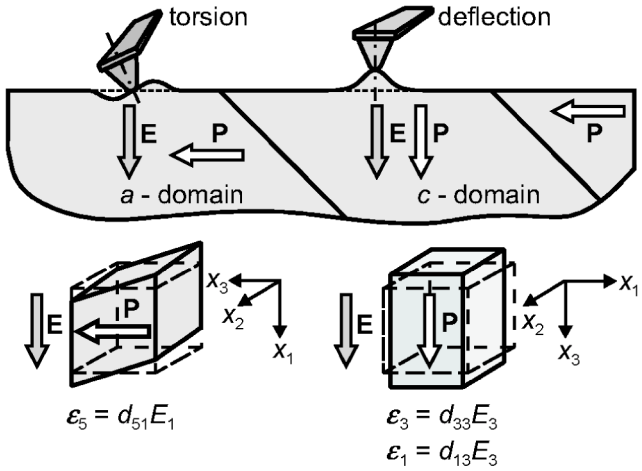

FIG. 1. Qualitative explanation of the contrast formation in PFM. The electric field induced from a conductive probe tip causes surface displacements due to the converse piezoelectric effect. Thus, an applied alternating voltage leads to surface vibrations which can be detected using conventional lock-in techniques.

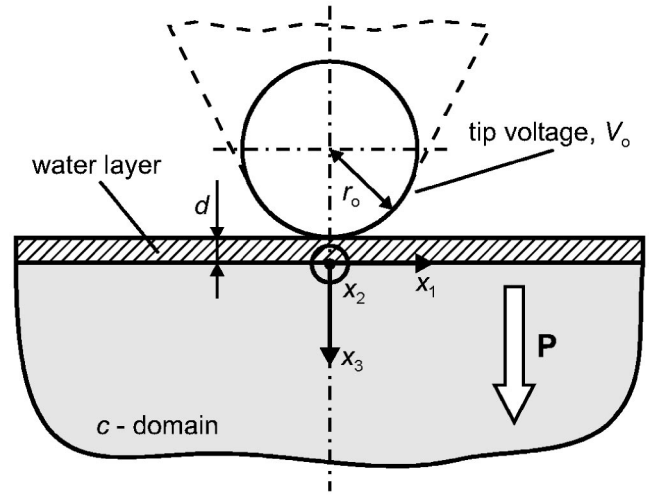

FIG. 2. Scheme of the probe tip situation. Here, r_0 is the radius of curvature of the tip, d the tip-surface separation distance, i.e., the thickness of the water layer, and x_i the introduced coordinate system used for the Green's function calculations.

pared with measured piezoresponse data of C^- domains from a $BaTiO_3$ bulk single crystal.

II. EXPERIMENTAL PROCEDURE

For the PFM measurement a commercial AFM (Digital Instruments, Dimension 3000, Nanoscope III) is used. We investigate an array of *a* and *c* domains of a $BaTiO_3$ bulk single crystal of approximately $5\times5\times5\ \mathrm{mm}^3$ in size. The crystal has been produced using the modified exaggerated grain growth method.[12] The characterized single crystal is oriented in the [001] direction plane, which has been determined in the scanning electron microscopy by electron backscattering diffraction and was subjected to compressive stresses parallel to the investigated surface. This procedure, which has been reported elsewhere,[13] gives rise to the formation and growth of needle shaped *c* domains and 90°-*ac*-domain walls. During the PFM measurements no mechanical stresses are applied. To generate the piezoelectric response signal, an alternating voltage of 20 kHz with an amplitude of up to $V_0=10$ V is applied to a conductive tip (Nanosensors, Pointprobe EFM). Using a lock-in amplifier, which is synchronized with the excitation signal, the amplitude of the first harmonic oscillation of the cantilever is separated from the deflection signal to obtain the out-of-plane piezoresponse dc signal P_{x3}. The corresponding surface displacement $\hat{u}_3$ can be calculated by

$$\hat{u}_3=\frac{S_{amp}}{S_{AFM}}\frac{P_{x_3}}{2}=S_{PFM}P_{x_3}, \tag{1}$$

where $S_{amp}=1$ mV/V, $S_{AFM}=11.7$ pm/V, and S_{PFM} are the sensitivities of the lock-in amplifier, the AFM detector, and the PFM sensitivity, respectively. The AFM detector is calibrated by means of the force-distance curve of the used probe. The displacement $\hat{u}_3$ is proportional to the half piezoresponse signal by convention since the lock-in amplifier probes the peak-to-peak value of the input signal.

III. METHODS FOR MODELING

The Green's function is used to compute the surface displacement of a *c* domain, which is oriented perpendicular to the surface. The domain is treated as a linear elastic isotropic and electrically anisotropic infinite half space, Fig. 2. The probe tip is approximated as a conductive sphere of an electrical potential V_0 and a diameter of $2r_0$ at a distance d from the surface. This distance takes the water layer into account, which is often present on a surface in an ambient environment.[14] Therefore the permittivity of the environment is set to $80\varepsilon_0$.

The electric field produced by the tip is computed using the image charge method.[15] The computation of the electric field distribution takes into account the high anisotropy of the $BaTiO_3$ *c* domain. The calculations illustrated in Fig. 3 are performed with MATHEMATICA[16] for a layer thickness of $d=1$ nm and the permittivity matrix $(\varepsilon_{11},\varepsilon_{33})=(4600,200)\varepsilon_0$ given by Merz.[17]

Green's function

Quasistatic conditions are assumed for the Green's function because the resonance frequency of the cantilever ($\approx$75 kHz) is much higher than the applied ac voltage of 20 kHz. In this approach the piezoelectric displacement is implemented into the nonpiezoelectric Green's function calculation using eigenstrains $d_{mnk}E_k$,[18] where d_{mnk} are the piezoelectric coefficients and $E_k=E_k(x')$ is the electric field strength distribution computed with the image charge method, as mentioned above. The out-of-plane displacement u_3 is then given by

$$u_3(\mathbf{x})=\int_{x_3=0}^{\infty}\int_{x_2=-\infty}^{\infty}\int_{x_1=-\infty}^{\infty}c_{jlmn}d_{mnk}E_k(x')\times\frac{\partial}{\partial x_l'}G_{3j}(\mathbf{x},\mathbf{x}')d\mathbf{x}', \tag{2}$$

Downloaded 20 Oct 2004 to 128.219.12.140. Redistribution subject to AIP license or copyright, see http://jap.aip.org/jap/copyright.jsp

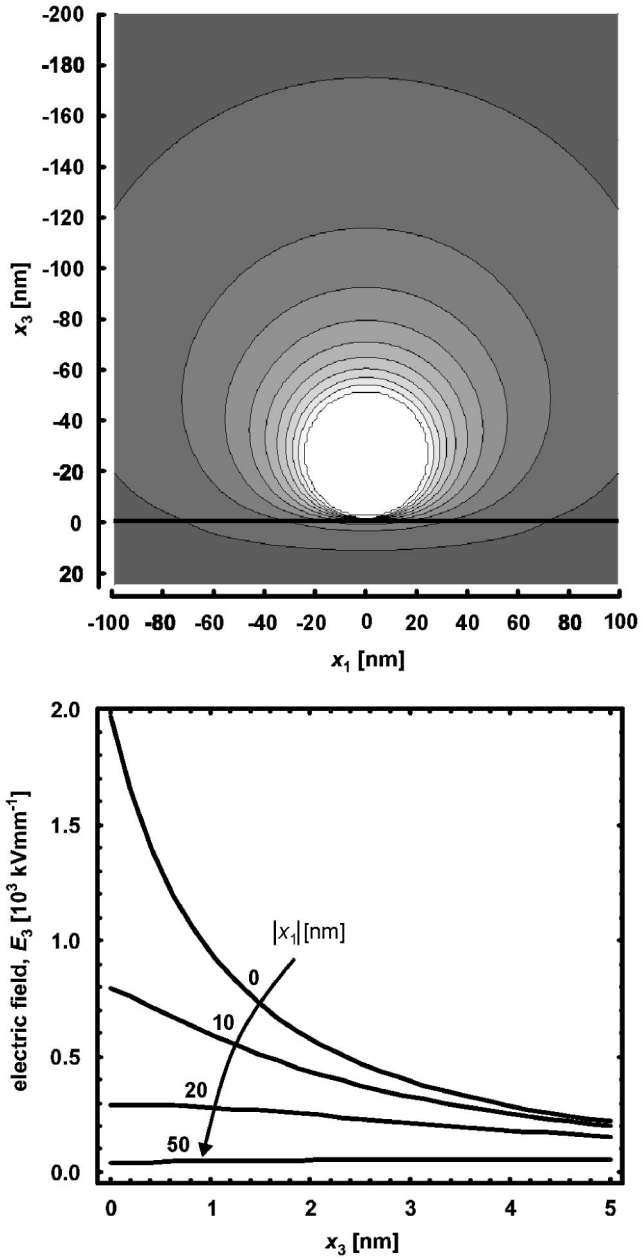

FIG. 3. Top: Potential distribution calculated for a tip-sample separation of $d=1$ nm. The distance of the equipotential lines is 1 V, starting with $V_0=10$ V at the central sphere. The tip radius is $r_0=25$ nm. Bottom: Electric field strength inside the c domain computed for different coordinates $|x_1|$.

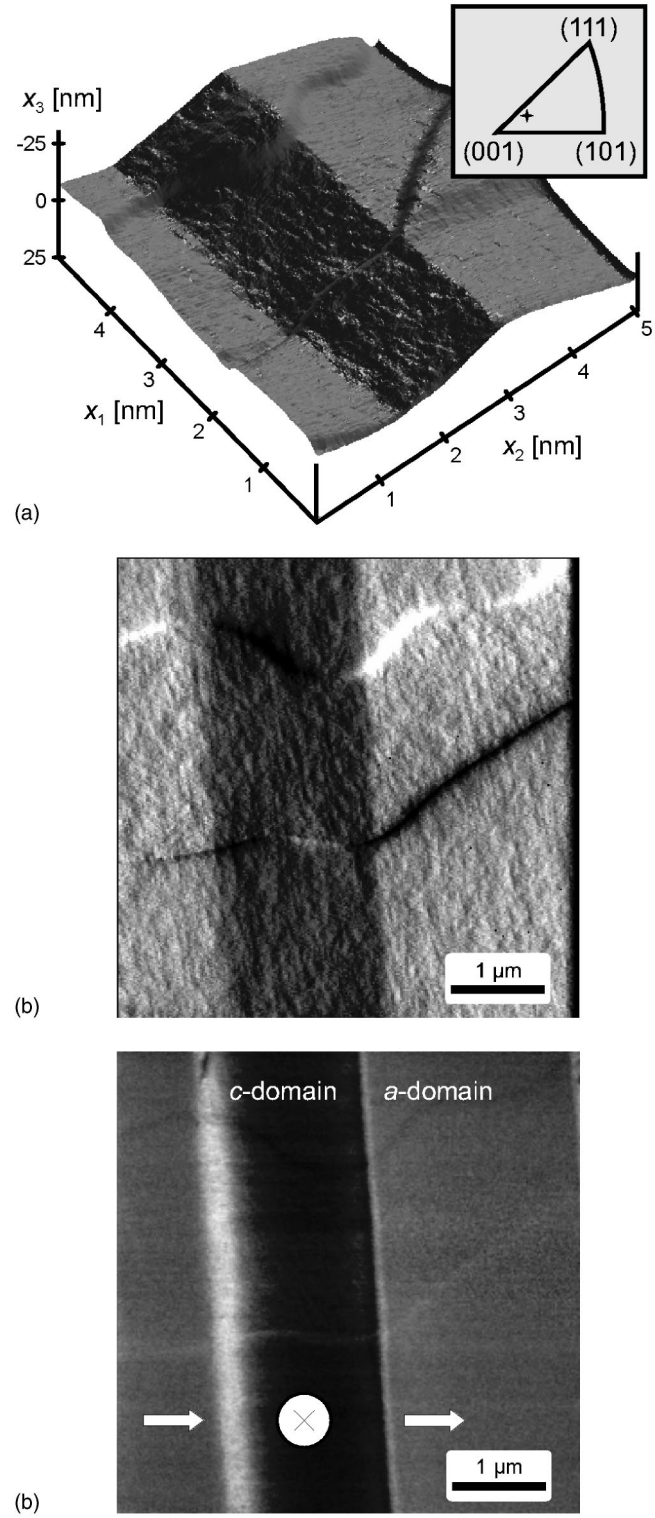

FIG. 4. AFM and PFM measurements of a $BaTiO_3$ single crystal. The topography is shown in a 3D plot (a) with the correspondent deflection image (b). The piezoresponse out-of-plane image (c) illustrates the observed array of *ac* domains. The crystal orientation is given by the stereographic representation shown in the insertion in (a).

where c_{jlmn} are the components of the elastic stiffness tensor for an isotropic material given as

$$c_{jlmn}=\frac{Y}{2(1-\nu)}\left[\frac{2\nu}{1-2\nu}\delta_{jl}\delta_{mn}+\delta_{jm}\delta_{jn}+\delta_{jn}\delta_{lm}\right], \quad (3)$$

where ν and Y are the Poisson ratio and the Young's modulus, respectively. Note that the Einstein summation convention is used. Equation (2) gives the displacements u in x_3 direction at the position $\mathbf{x}$ inside the infinite half space $x_3>0$ due to the stress state based on the eigenstrains described in the coordinate system $\mathbf{x}'$. The link between the stress and displacement field is realized by the Green's function $G_{3j}(\mathbf{x},\mathbf{x}')$. Since we are only interested in the displacements at the surface, $x_3=0$, a corresponding Green's function for a semi-infinite isotropic dielectric medium is utilized as given by Mura,[18] Eq. (4),

Downloaded 20 Oct 2004 to 128.219.12.140. Redistribution subject to AIP license or copyright, see http://jap.aip.org/jap/copyright.jsp

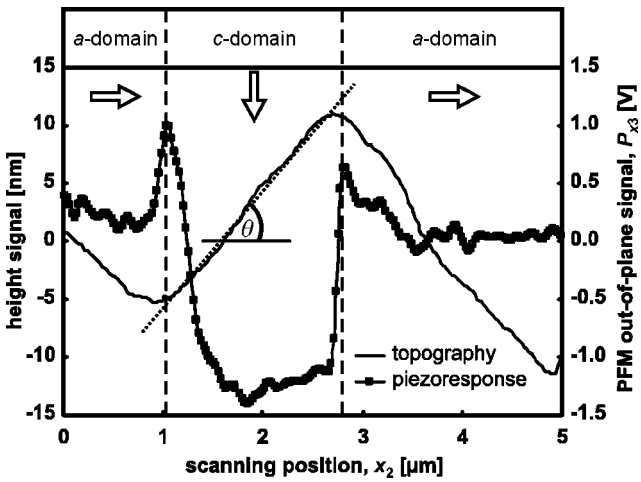

FIG. 5. Section scans of the height and PFM image (see Fig. 4). The surface displacements $\hat{u}_3$ are calculated from the PFM signals P_{x3}. The PFM scan corresponds well with the topography which allows identifying the sketched *ac*-domain array.

$$G_{ij}(\mathbf{x},\mathbf{x}') = \frac{1+\nu}{2\pi Y}\left[\frac{\delta_{ij}}{R} + \frac{(x_i - x_i')(x_j - x_j')}{R^3} + \frac{1-2\nu}{R+x_3'}\left(\delta_{ij} - \frac{(x_i - x_i')(x_j - x_j')}{R(R+x_3')}\right)\right],$$

$$R = \sqrt{(\mathbf{x}-\mathbf{x}')^2}. \tag{4}$$

A Poisson ratio $\nu = 0.35$ is used, which is measured for a $BaTiO_3$ polycrystal. The integral in Eq. (2) is independent of Young's modulus. The piezoelectric coefficients for a $BaTiO_3$ single crystal are $(d_{33}, d_{31}, d_{15}) = (0.0856, 0.0345, 0.3920)$ nm/V.[19] Unless otherwise stated, the tip radius is $r_0 = 25$ nm and the amplitude of the tip voltage is $V_0 = 10$ V.

IV. RESULTS AND DISCUSSION

A. Measurement of the piezoelectric displacement

The surface of the investigated bulk $BaTiO_3$ single crystal is almost exactly a {001} crystallographic. This is shown in the stereographic representation in the upper right corner of Fig. 4(a). Figure 4 also shows the imaged area over $5 \times 5\ \mu m^2$ in AFM, where the topography is represented by the three-dimensional and the deflection image, Figs. 4(a) and 4(b). The corresponding piezoresponse image with the out-of-plane signal P_{x3} is shown in Fig. 4(c).

Due to the compressive stress applied to the $BaTiO_3$ single crystal during sample preparation, needle shaped *c* domains are created. These correspond to {110} domain walls of the pseudocubic $BaTiO_3$ lattice according to the known crystal orientation from the stereographic analysis. A section scan of the investigated surface area shows a sawtooth curve of the height profile, Fig. 5. The tilt angle θ is determined to be $0.59° \pm 0.01°$, which corresponds very well with the theoretical value of 0.60° for a 90°-*ac*-domain wall calculated from the tetragonal distortion of $BaTiO_3$ at room temperature, i.e., $c/a = 1.01$.[20]

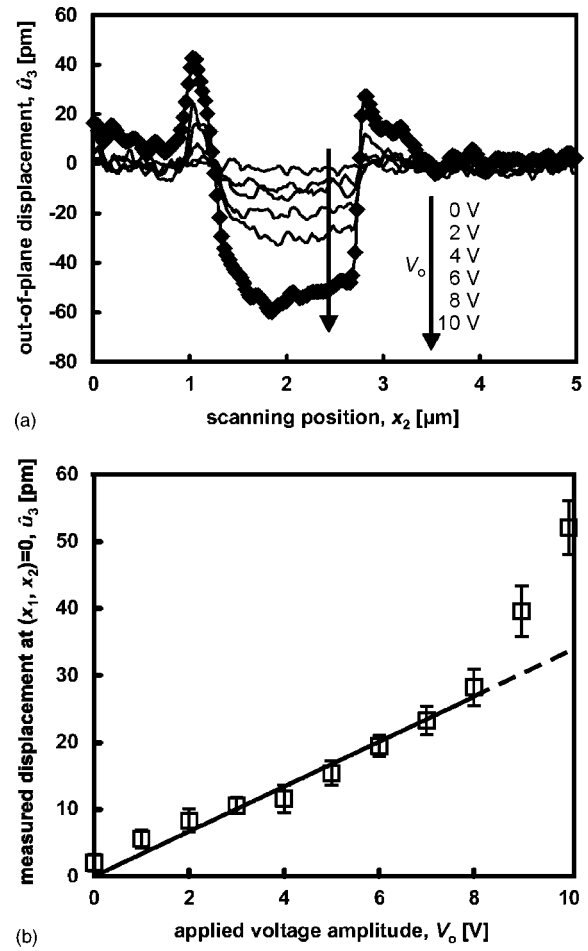

FIG. 6. Section scans of the out-of-plane surface displacements of the *ac*-domain array as a function of the applied tip voltage V_0. The depth of the well increases with increasing tip voltage (a). Averaging the values inside the well from $x_2 = 1.5$ to 2.5 μm gives the PFM sensitivity of the C^- domain (b). The response is linear up to $V_0 = 8$ V.

The section scan of the piezoresponse signal P_{x3} shows a well profile characteristic of a C^- domain, Fig. 5. The maximum and minimum value of the height signal correlate with the borders of the well in the piezoresponse image. Therefore, we have the situation of a C^- domain surrounded by *a* domains. The PFM signal is close to zero within the *a* domain. The orientation of the *a* and *c* domains can be evaluated from the phase shift of the lock-in amplifier.[8] Figure 6(a) gives the results of the out-of-plane displacements $\hat{u}_3$ calculated from the piezoresponse signal using Eq. (1). The depth of the well inside the *c* domain increases with increasing applied voltage V_0. Averaging the well depth from $x_2 = 1.5$ to 2.5 μm leads to the curve shown in Fig. 6(b), which shows the out-of-plane piezoresponse displacement $\hat{u}_3$ as a function of the applied voltage amplitude. The error bars represent the standard deviation of the same interval. The response revealed a linear behavior up to a voltage of approx. $V_0 = 8$ V with a sensitivity of $S_{PFM} = \partial \hat{u}_3 / \partial V_0 = 3$ pm/V. For higher voltages the signal shows a progressive trend.

B. Modeling piezoresponse of *c* domains

For the described situation of a charged sphere in contact with an infinite *c* domain (Fig. 2), the surface displacement

Downloaded 20 Oct 2004 to 128.219.12.140. Redistribution subject to AIP license or copyright, see http://jap.aip.org/jap/copyright.jsp

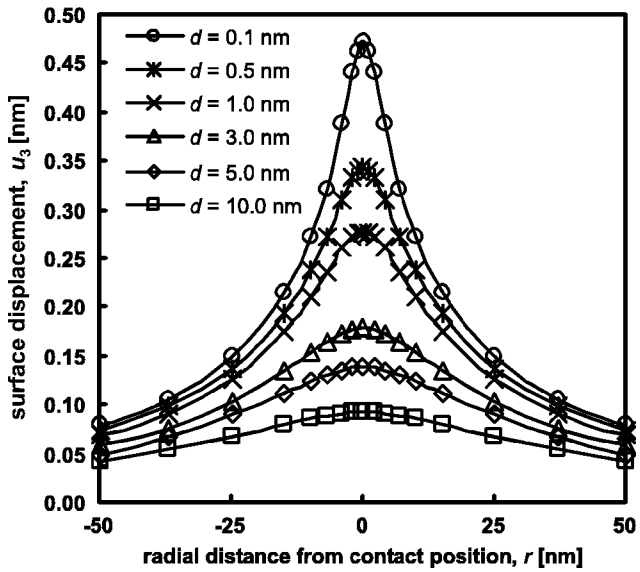

FIG. 7. Surface displacements u_3 vs the radial distance from the contact position $r=\pm\sqrt{x_1^2+x_2^2}$ computed with the Green's function solution for the situation described in Fig. 2. The tip voltage is $V_0=10$ V. The maximum displacement $\hat{u}_3$ decreases with increasing tip-sample separation d.

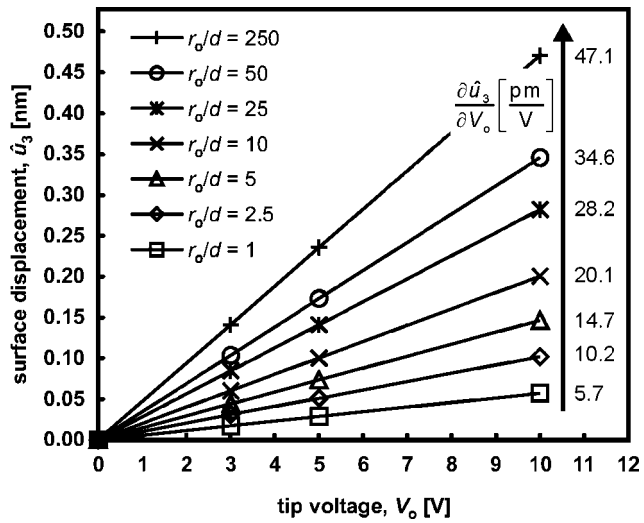

FIG. 8. Maximum surface displacements $\hat{u}_3$ as a function of the applied tip voltage V_0. The PFM sensitivity strongly depends on the ratio r_0/d.

in x_3 direction, u_3, is calculated using the Green's function, Eq. (2). For the sake of convenience, the solution is converted to cylindrical coordinates and the integration radius is limited to $r=500$ nm. By means of numerical convergence analysis, the final accuracy of this approximation is determined to be $\Delta u_3<2$ pm.

Figure 7 illustrates the result of the surface displacement profiles for different tip-sample separation distances d. The calculations are performed with $r_0=25$ nm and $V_0=10$ V. For negative excitation voltages or opposite polarization of the c domain (C^+) the shape of the profile remains unchanged but the displacements are negative. The radius of curvature directly underneath the peak is calculated using a sphere function fitted through three adjacent points around the center. Note that due to the aspect ratio used in Fig. 7 the curvature appears to be highly exaggerated. The resulting surface curvature is always larger than that of the tip r_0 even when the tip sample separation is close to zero (also see Fig. 9). Hence, the PFM signal is composed of both the negative and positive half waves of the excitation voltage, as asserted in Eq. (1).

To compare the computation with the PFM measurements, the maximum surface displacement at the contact position, i.e., $(x_1,x_2)=\mathbf{0}$, $\hat{u}_3$, must be evaluated. Figure 8 illustrates the results for a variety of ratios r_0/d as a function of the tip voltage V_0. The ratio r_0/d controls the sensitivity. As expected from the used linear constitutive law, the displacements are directly proportional to the electric potential. The dependence of the sensitivity with respect to the tip-sample separation is illustrated in Fig. 9 for a tip radius of $r_0=25$ nm. The maximum value is obtained for direct contact, namely, $\partial\hat{u}_3/\partial V_0=56.6$ pm/V. This value remains unchanged even under dry conditions represented by a permittivity of the environment of ε_0.

The measured sensitivity of $\partial\hat{u}_3/\partial V_0\approx 3$ pm/V would be obtained for a ratio of $r_0/d<1$, which corresponds to a water layer of $\approx$20–50 nm for reasonable tip radii. This is in agreement with experimental results by Freund *et al.*[14] who investigated layer thicknesses on gold, titanium, and graphite. For instance, scanning tunneling microscopy measurements on Ti show that within the interval 20%–50% humidity the related layer thickness increases linearly from 50 to 100 nm. The authors argue that this strong water adsorption is based on an oxide layer on the Ti surface. Thus, it seems quite probable that on the $BaTiO_3$ surface such water layer thicknesses are possible as well. The very high electric field inside the material in the vicinity of the tip as shown in Fig. 3 gives rise to another explanation. Since the coercive field of $BaTiO_3$ is small, the high fields might lead to reorientation of domains in the contact region. If fully 180° domain

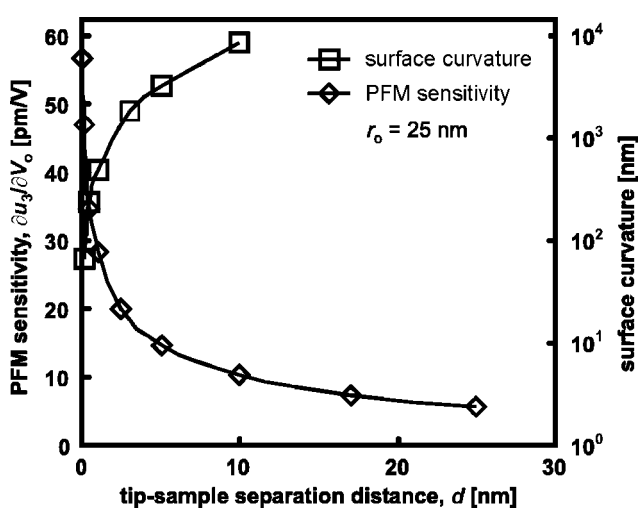

FIG. 9. PFM sensitivities and the radius of curvature of the surface at $(x_1,x_2)=\mathbf{0}$ calculated for a tip radius $r_0=25$ nm. The PFM sensitivity increases with decreasing tip-sample separation until a maximum value $\partial u_3/\partial V_0=56.6$ pm/V is reached for direct contact. The radius of curvature of the surface at the maximum is always larger than the tip radius. Thus, the inverted peak fully contributes to the PFM signal during ac excitation.

Downloaded 20 Oct 2004 to 128.219.12.140. Redistribution subject to AIP license or copyright, see http://jap.aip.org/jap/copyright.jsp

switching is assumed, the sensitivity would decrease by a factor of 2 only, because the polarization vector is fully coupled with the electric field and thus the piezoelectric response is always positive. Obviously, full reorientation does not take place because contrast formation in 180° out-of-plane domain arrays is observed in PFM, but domain switching might reduce the sensitivity slightly. Among the simplifications of the utilized model, i.e., the spherical approximation of the probe tip and, in particular, the infinite domain size, wear of the used Pt/Ir-coated tip could strongly decrease the sensitivity as well. Lin *et al.*[21] showed that the difference between a high-quality Au-coated tip and a non-coated doped silicon tip can influence the PFM sensitivity by a factor of 10.

However, even under dry conditions, the maximum sensitivity, computed to be 57 pm/V, is significantly smaller than one would expect for an unconstrained *c* domain under uniform electric field, i.e., $d_{33}=86$ pm/V. This indicates that the complex electrostatic tip-sample interaction is predominant for bulk characterization and prohibits a simple evaluation of the piezoelectric properties of the material.

V. CONCLUSIONS

(i) We present three-dimensional elastic Green's function calculations with a piezoelectric eigenstrain applied to compute the out-of-plane surface displacements of a bulk $BaTiO_3$ single crystal in piezoresponse mode.

(ii) The PFM displacements measured within the $BaTiO_3$ *c* domain increase linearly with the applied voltage, which is reproduced by the Green's function calculations. The measured displacement matches the computation when a water layer thickness of ≈20–50 nm is assumed.

(iii) The computed PFM sensitivities are distinctively smaller than the d_{33} value of the $BaTiO_3$ single crystal. This signifies that opposite to thin films the complex electrostatic tip-sample interaction is predominant for piezoelectric bulk materials and prohibits a simple evaluation of the piezoelectric properties of the material.

ACKNOWLEDGMENTS

The authors acknowledge financial support by the German Research Foundation (DFG) and the research performed as a Eugene P. Wigner Fellow and staff member at the Oak Ridge National Laboratory, managed by UT-Battelle, LLC, for the U.S. Department of Energy under Contract No. DE-AC05-00OR22725 (S.V.K.).

[1] H. Birk, J. Glatz-Reichenbach, L. Jie, E. Schreck, and K. Dransfeld, J. Vac. Sci. Technol. B **9**, 1162 (1991).
[2] P. Guthner and K. Dransfeld, Appl. Phys. Lett. **61**, 1137 (1992).
[3] K. Franke, J. Besold, W. Haessler, and C. Seegbarth, Surf. Sci. Lett. **302**, 1283 (1994).
[4] A. Gruverman, O. Auciello, and H. Tokumoto, J. Vac. Sci. Technol. B **14**, 602 (1996).
[5] A. Gruverman, O. Auciello, R. Ramesh, and H. Tokumoto, Nanotechnology **8**, A38 (1997).
[6] M. Ablanalp, L. M. Eng, and P. Günter, Appl. Phys. A: Mater. Sci. Process. **66**, 5231 (1998).
[7] L. M. Eng, M. Ablanalp, and P. Günter, Appl. Phys. A: Mater. Sci. Process. **66**, 5679 (1998).
[8] L. M. Eng, H.-J. Güntherodt, G. A. Schneider, U. Köpke, and J. Muñoz Saldaña, Appl. Phys. Lett. **74**, 233 (1999).
[9] S. V. Kalinin and D. A. Bonnell, Phys. Rev. B **65**, 125408 (2002).
[10] M. Schvebelman, P. Urenski, R. Shikler, G. Rosenman, Y. Rosenwaks, and M. Molotskii, Appl. Phys. Lett. **80**, 10 (2002).
[11] E. Karapetian, I. Sevostianov, and K. Kachanov, Philos. Mag. B **80**, 3 (2000).
[12] J. Muñoz-Saldaña, B. Mullier, and G. A. Schneider, J. Eur. Ceram. Soc. **22**, 681 (2002).
[13] J. Muñoz-Saldaña, G. A. Schneider, and L. M. Eng, Surf. Sci. Lett. **480**, L402-10 (2001).
[14] J. Freund, J. Halbritter, and J. K. H. Hörber, Microsc. Res. Tech. **44**, 327 (1999).
[15] J. D. Jackson, *Classical Electrodynamics*, 2nd ed. (Wiley, New York, 1975).
[16] MATHEMATICA, Version 3.0, Wolfram Research Inc., Champaign, Illinois.
[17] W. J. Merz, Phys. Rev. **76**, 1221 (1949).
[18] T. Mura, *Micromechanics of Defects in Solids* (Martinus Nijhoff, Dordrecht, 1987).
[19] D. Berlincourt and H. Jaffe, Phys. Rev. B **111**, 143 (1958).
[20] H. H. Rogers, MIT Technical Report No. 56, 1952.
[21] H.-N. Lin *et al.*, J. Vac. Sci. Technol. B **21**, 916 (2003).

Downloaded 20 Oct 2004 to 128.219.12.140. Redistribution subject to AIP license or copyright, see http://jap.aip.org/jap/copyright.jsp